A CT Scan Harmonization Technique to Detect Emphysema and Small Airway Diseases

Gonzalo Vegas-Sánchez-Ferrero(✉) and Raúl San José Estépar

Applied Chest Imaging Laboratory (ACIL), Brigham and Women's Hospital, Harvard Medical School, Boston, MA, USA
{gvegas,rsanjose}@bwh.harvard.edu

Abstract. Recent studies have suggested the central role of small airway destruction in the pathogenesis of COPD leading to further parenchymal destruction. This evidence has sparked the interest in in-vivo assessment of small airway disease overall at the early onset of the disease. The parametric response mapping (PRM) technique has been proposed to distinguish gas trapping due to small airway disease from low attenuation areas due to emphysema. Despite its success, the PRM technique shows some limitations that are precluding the interpretation of its results. The density value used to assess gas trapping highly depends on acquisition parameters, such as dose and reconstruction kernel, and changes in body size, that introduce inhomogeneous photon absorption patterns. In particular, many studies using PRM employ inspiratory and expiratory images that are obtained at different dose levels. Emphysema impact in early disease may be confounded with the gas trapping due to the noise introduced by differences in the acquisition during the PRM. In this work, we propose a CT harmonization technique to remove the nuisance factors to distinguish between small airway disease and emphysema. Our results show that the measurements based on CT harmonization provide an increase in the detection of both emphysema and airway disease, resulting in a statistically significant impact of both components and a better association with lung function measures.

Keywords: CT scans · Emphysema · Lung disease
Statistical characterization

1 Introduction

Chronic Obstructive Pulmonary Disease (COPD) is a complex syndrome with widely varying clinical and imaging characteristics. The chronic airflow limitation of COPD is caused by a mixture of small airway disease and parenchymal

This study was supported by the National Institutes of Health NHLBI awards R01HL116931, R01HL116473 and R21HL140422.

D. Stoyanov et al. (Eds.): RAMBO 2018/BIA 2018/TIA 2018, LNCS 11040, pp. 180–190, 2018.
https://doi.org/10.1007/978-3-030-00946-5_19

destruction (emphysema). COPD is a major cause of morbidity and mortality. Despite declines in smoking, mortality from COPD continues to increase and is now the third leading cause of death in the US. Recent studies have suggested that the central role of small airway disease in the pathogenesis of COPD leads to additional parenchymal destruction [1]. This evidence has sparked the interest in in-vivo assessment of small airway disease overall at the early onset of the disease.

Computed Tomography (CT) is the main imaging modality for thoracic conditions due to its high tissue-air contrast. CT has been proven to be effective in the quantification of emphysema [2]. However, direct measurements of the dimensions of small airways using CT scanning is beyond current imaging resolution [3]. One option to indirectly assess the effects of smaller airways is to quantify gas trapping by measuring the percent of voxels in the lung lower than -856 Hounsfield Units (HU) on an expiratory CT scan [4]. A technique named Parametric Response Mapping (PRM) has been proposed to distinguish gas trapping due to small airway disease from low attenuation areas due to emphysema [5]. The technique employs both inspiratory and expiratory CT scans. After the co-registration of both images and the application of established CT density thresholds, one can distinguish between functional small airway disease (FSAD) and emphysema.

The COPD imaging community has extensively used PRM since its introduction. However, despite its success, the PRM technique shows some limitations that are precluding the interpretation of its results. The density value used to assess gas trapping highly depends on acquisition parameters, such as dose and reconstruction kernel, and changes in body size, that introduce inhomogeneous photon absorption patterns. In particular, many studies using PRM employ inspiratory and expiratory images that are obtained at different dose levels and introduce a spatially variant noise and bias across the image [6]. These effects are nuisance factors that affect the inter-scanner and inter-subject variability in CT density and confounds CT-derived metrics by PRM. As an example, Fig. 1 shows the expiratory and inspiratory scans of the same subject and the local

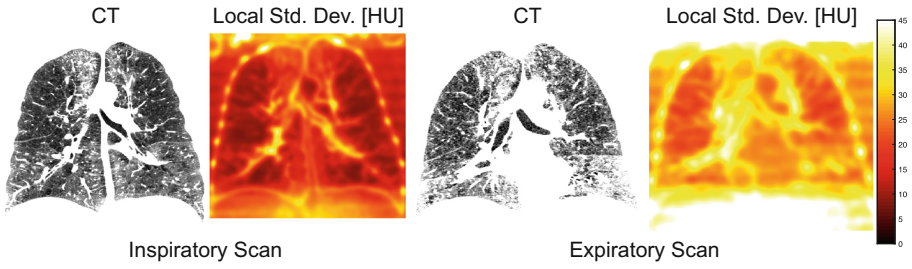

Fig. 1. Inspiratory and expiratory scans used for PRM analysis. Note that the noise variance remarkably increases in the expiratory scan due to the lower dose applied. Additionally, the noise changes across the image affecting the PRM analysis.

standard deviation in each image. Note that the noise changes across the image and that the expiratory scan shows a higher variance of noise due to the lower dose applied.

Researchers are aware of the importance of these nuisance factors and much effort has been done in reducing the spatially variant noise for both iterative and back projection reconstruction techniques [7,8]. Spatial discrepancies in the attenuation levels have been largely observed in clinical studies, especially for air [9]. Some approaches using anatomical references like trachea and aorta densities have been proposed with promising results [9–11]. The inter-scanner deviations due to calibration are also an important factor that has been studied in [12].

A recent PRM study has successfully associated functional respiratory decline with FSAD in the mild-moderate stage of COPD [13]. Surprisingly, the emphysema in this early stage has no effect. The detection of FSAD has been useful in the early detection of rapid lung function decline. However, if the mentioned nuisance factors that affect the interpretation of PRM are precluding the distinction between FSAD and emphysema, we could be losing valuable information about the emphysema and FSAD interplay that can help identify trajectories of rapid decline.

In this work, we propose a harmonization methodology that simultaneously minimizes the spatially variant noise and biases. We employ the harmonization in both inspiratory and expiratory scans for the PRM analysis. Results show that our technique is able to detect the impact of both emphysema and airway disease in contrast to other reference methods used to palliate the effect of noise. Correlation analyses with lung function show a better fit with the harmonized data that cannot be achieved with other conventional noise reduction methodologies. This result evidences the importance of scan harmonization for clinical data and shows that the role of emphysema is still significant in early disease and can be distinguished from FSAD.

2 Harmonization of CT Scans

The harmonization of CT scans will be performed in three steps. First, we estimate the spatially variant noise power and signal. Second, we remove the spatially variant bias induced by the noise, and finally the density levels are re-calibrated to the nominal values of apparent anatomical structures.

Characterization of Tissues. The estimation of both the signal and noise components of the CT image is performed by adopting the statistical characterization of signal/noise in CT scans proposed in [8]. We adopted this model because it offers a versatile methodology to describe the spatially variant noise in CT scans reconstructed with both backprojected and iterative methods without the need of sinograms or any interaction with the reconstruction method.

This model consists in a non-central Gamma distribution (nc-Γ) for each voxel $X(\boldsymbol{r})$ of the image:

$$f_X(x|\alpha,\beta,\delta) = \frac{(x-\delta)^{\alpha-1}}{\beta^\alpha \Gamma(\alpha)} e^{-\frac{x-\delta}{\beta}}, \qquad x \geq \delta \text{ and } \alpha,\beta > 0 \tag{1}$$

where α, β are the spatially variant shape, scale parameters; and δ is location parameter usually set to the minimum value of the CT scan (usually -1024 HU).

The heterogeneous nature of lung parenchyma is effectively described by means of a mixture model of nc-Γ distributions:

$$p(x(\boldsymbol{r})) = \sum_{j=1}^{J} \pi_j(\boldsymbol{r}) f_X(x(\boldsymbol{r})|\alpha_j(\boldsymbol{r}),\beta_j(\boldsymbol{r}),\delta) \tag{2}$$

for J components, where π_j are the weights of the mixture and α_j, β_j the parameters of each component. To ensure that the heterogeneous composition of the lung is properly described in the mixture model, we set J = 9 components from -1000 to 400 HU. This is a reasonable range of attenuations considering that the normal lung attenuation is between -600 and -700 HU, and also allows us to model other tissues within the CT image such as vasculature, muscle, fat or bone.

The estimation of the parameters for each component is achieved through the Expectation-Maximization method for known mean values for each component, $\{\mu_j\}_{j=1}^J$, which reduces the problem to solve a non-linear equation in each iteration at each location. The estimation of the shape parameters for each component, α_j, are obtained for each location $\boldsymbol{r}$ by solving the following non-linear equation derived from the maximum likelihood estimation in the local neighborhood $\eta(\boldsymbol{r})$ (see [8] for more details):

$$\log(\alpha_j(\boldsymbol{r})) - \psi(\alpha_j(\boldsymbol{r})) = \frac{\sum\limits_{s\in\eta(r)} \gamma_j(\boldsymbol{s}) \dfrac{x_i(\boldsymbol{s})-\delta}{\mu_j}}{\sum\limits_{s\in\eta(r)} \gamma_j(\boldsymbol{s})} - \frac{\sum\limits_{s\in\eta(r)}^{N} \gamma_j(\boldsymbol{s}) \log\left(\dfrac{x_i(\boldsymbol{s})-\delta}{\mu_j}\right)}{\sum\limits_{s\in\eta(r)} \gamma_j(\boldsymbol{s})} - 1 \tag{3}$$

with $\psi(\cdot) = \Gamma'(x)/\Gamma(x)$ being the digamma function, and $\gamma_j(\boldsymbol{r}) = P(j|x(\boldsymbol{r}))$ are the posterior probabilities for the j-th tissue class at location $\boldsymbol{r}$:

$$\gamma_j(\boldsymbol{r}) = \frac{\pi_j(\boldsymbol{r}) f_X(x(\boldsymbol{r})|\alpha_j(\boldsymbol{r}),\beta_j(\boldsymbol{r}),\delta)}{\sum_{k=1}^{J} \pi_k(\boldsymbol{r}) f_X(x(\boldsymbol{r})|\alpha_k(\boldsymbol{r}),\beta_k(\boldsymbol{r}),\delta)}. \tag{4}$$

Then, the scale factor is calculated as $\beta_j = \mu_j/\alpha_j$ and the priors π_j are updated as $\pi_j = \frac{1}{N}\sum_{i=1}^{N} \gamma_{i,j}$.

Equations (3 and 4) are iteratively applied until convergence is reached. This convergence is usually achieved in very few iterations due to the constraint imposed by the mean $\{\mu_j\}_{j=1}^J$ for each tissue. A suitable initialization of parameters for the iterative optimization is $\pi_j = 1/J$, $\alpha_j = 2$ and $\beta_j = \mu_j/\alpha_j$ for each component.

Estimation of the Signal and Local Variance of Noise. The characterization of tissues allows us to calculate the sample conditioned moments to each tissue class as follows:

$$\langle X^k(\mathbf{r})|j\rangle = \frac{\sum_{\mathbf{s}\in\eta(\mathbf{r})} x(\mathbf{s})^k \gamma_j(\mathbf{s})}{\sum_{\mathbf{s}\in\eta(\mathbf{r})} \gamma_j(\mathbf{s})}. \tag{5}$$

This formulation provides a more robust estimate of conditioned local moments since it just considers the samples belonging to the j-th tissue class.

Finally, the moments for each location can be calculated as the weighted average of the conditioned moments as:

$$E\{X(\boldsymbol{r})^k\} = \sum_{j=1}^{J} \pi_j(\boldsymbol{r}) E\{X(\mathbf{r})^k|j\} \approx \sum_{j=1}^{J} \pi_j(\boldsymbol{r}) \langle X(\boldsymbol{r})^k|j\rangle. \tag{6}$$

Correction of Spatially Variant Bias. The estimation of the local mean $E\{X(\boldsymbol{r})\}$ and local variance of noise $\widehat{\sigma}^2(\boldsymbol{r}) = E\{X^2(\boldsymbol{r})\} - E\{X(\boldsymbol{r})\}^2$ allow us to remove any bias derived from the noise. This bias has been previously reported in the literature [9–11]. As an example of this effect, in Fig. 2a we show the linear dependence between local mean and local variance.

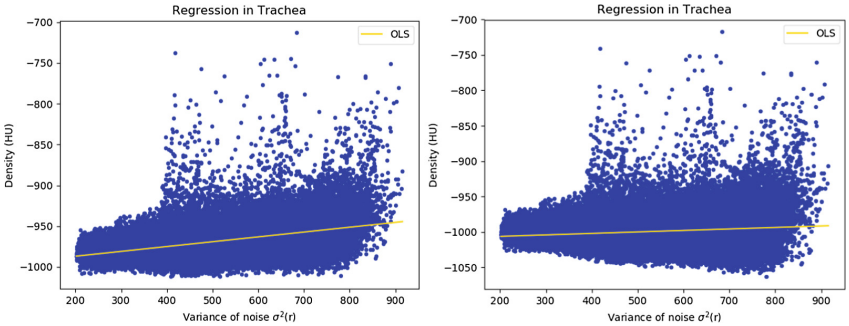

a) Original b) Calibrated

Fig. 2. Linear regression between local mean and local variance in the trachea before and after calibration.

This dependence is corrected by estimating the linear coefficient of the ordinary least squares (OLS) linear regression, β, in the trachea. This coefficient decreases as the tissue becomes denser as a consequence of the more symmetric distribution of tissues with higher attenuation value than the lung (blood, fat, bone).

One of the advantages of adopting the noise model of Eq. 2 is that there is a functional relationship between the linear coefficient and the CT number: $\beta(\mu) = K/(\mu - \delta)$, where μ is the attenuation coefficient and K is a constant to

be determined [11]. In this work, we take advantage of the linear regression in the trachea to determine K. This way, the linear coefficient becomes:

$$\beta(\mu) = \begin{cases} \beta_{\text{trachea}} \dfrac{\mu_{\text{trachea}} - \delta}{\mu - \delta} & \text{if } \mu > \mu_{\text{trachea}} \\ \beta_{\text{trachea}} & \text{if } \mu \leq \mu_{\text{trachea}} \end{cases} \tag{7}$$

where μ_{trachea} is the mean value of samples in the trachea. Now, the spatially variant bias can be removed as follows:

$$\widetilde{X}(\boldsymbol{r}) = E\{X(\boldsymbol{r})\} - \beta\left(E\{X(\boldsymbol{r})\}\right)\widehat{\sigma}^2(\boldsymbol{r}) \tag{8}$$

It is important to note that a systematic bias still can be present in the image since Eq. (8) removes the linear relationship with the local variance, but not the intercept. We remove the intercept by adjusting the mean values to the nominal densities of tissues in anatomical references. The most evident structures are the descending aorta, (Ω_{aorta}), where the blood attenuation level ($\mu_{\text{blood}} = 50$ HU) is usually adopted [10]; and the trachea, (Ω_{trachea}), where the air is set to $\mu_{\text{air}} = -1000$ HU by definition. Then, the harmonized image is obtained by linear interpolation for those attenuation levels:

$$\widehat{X}(\boldsymbol{r}) = (1\text{–}\lambda(\boldsymbol{r}))\mu_{\text{air}} + \lambda(\boldsymbol{r})\mu_{\text{blood}}; \text{ with } \lambda(\boldsymbol{r}) = \frac{\widetilde{X}(\boldsymbol{r}) - E\left\{\widetilde{X}(\boldsymbol{r})|\Omega_{\text{trachea}}\right\}}{E\left\{\widetilde{X}(\boldsymbol{r})|\Omega_{\text{aorta}}\right\} - E\left\{\widetilde{X}(\boldsymbol{r})|\Omega_{\text{trachea}}\right\}} \tag{9}$$

We show in Fig. 2b the effect of harmonization in the trachea. Note that the linear relationship between the variance of noise and the attenuation level is effectively removed by Eq. (8). Additionally, the intercept is also corrected to the nominal value for air (−1000 HU).

3 Experiments and Results

The PRM study was performed in a set of 48 inspiratory and expiratory scan pairs acquired in the same session from subjects with diagnosed COPD with a range of severity levels. 5 Different devices from 2 different manufacturers were used: GE VCT-64, Siemens Definition Flash, Siemens Definition, Siemens Sensation-64, and Siemens Definition AS+. The doses for the inspiratory and expiratory scans were 200 mAs and 50 mAS respectively in all the acquisitions. Expiratory scans are typically done at a lower dose to reduce total radiation exposure resulting in an increased image noise. The discrepancy in doses implies that different responses in the spatial noise variance and biases (as in Fig. 1).

The assessment of the harmonization technique here proposed was performed by comparing its performance to other reference methods that are commonly used to reduce the effects of noise in medical imaging. We considered the median filter and the non-local means filter as the reference methods for comparison. The median filter has been widely used in the CT imaging community for denoising

purposes due to the little assumptions about the underlying noise model [14]. We used two median filters with $3\times3\times3$ (Median1) and $5\times5\times5$ (Median2) voxels window respectively. We also chose the non-local means filter (NLM) since it has shown to be an effective filtering technique in multiple modalities [15]. We use the implementation presented in [16] because of its efficiency for 3D volumes. The main parameter of this approach is the noise power. To perform a fair comparison, we estimated the noise power for each case using the same approach that we used in the CT harmonization. After filtering the image with our approach and the reference methods, we computed the percentage of emphysema (Emph%) and FSAD (FSAD%) using the same PRM technique for all the methods (we applied the -950 HU and -856 HU thresholds for inspiratory and expiratory scans as suggested in [5]).

Comparison Between Methods. We performed a population analysis of the difference of emphysema% and FSAD% across the different methods comparing means and concordance between methods. Figure 3a–b show the distributions of emphysema% and FSAD%, where our approach yields a mean score statistically higher to the other methods in pairwise comparisons using Dunn's method for joint ranking (p-value $< 10^{-4}$). The reference methods do not show significant differences among them or even with respect to the original. This discrepancy between the harmonized data with respect to the reference methods and the original image is due to the better detection of emphysema and FSAD. This can be easily confirmed by visual inspection in Fig. 3c–d, where the PRM analysis of a subject with an evident emphysema region is represented for the original and

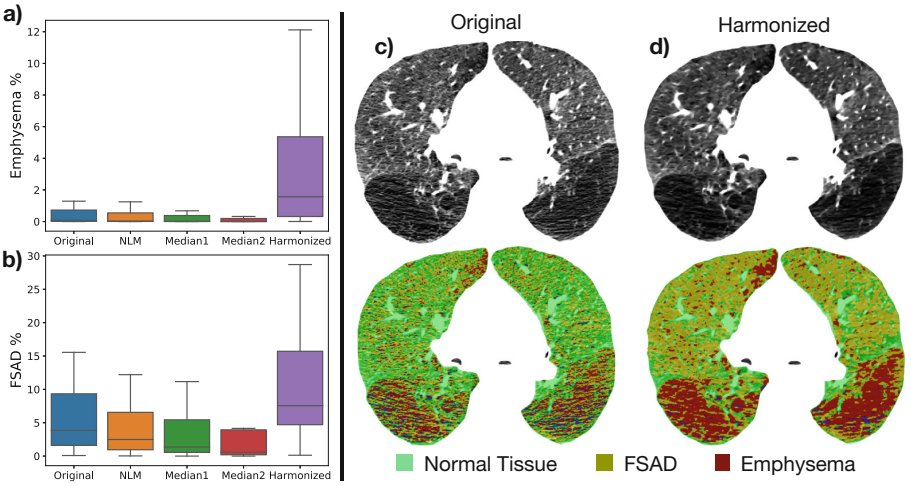

Fig. 3. Left: Distribution of Emph% (a) and FSAD% (b) in the analyzed population across filtering methods. The proposed harmonization approach increased the ability to resolve more emphysema and small airway disease. Right: PRM analysis for the inspiratory scans; original (c) and harmonized (d).

harmonized data. Note that the PRM overestimates the normal tissue because of the noise influence. Conversely, the harmonization mitigates the noise effect in regions of parenchyma and massive emphysema which, in turn, leads to a more accurate measure of emphysema and FSAD. This result suggests that a reduction of noise with the methods available in the literature does not provide a statistically significant difference with the original image when measuring FSAD or emphysema. To confirm this fact, we performed a concordance analysis using the so-called *Concordance Correlation Coefficient* (CCC) proposed by Lin [17], a widely accepted index of agreement in settings with different raters. This measure assumes a positive correlation between raters, is bounded in $[0, 1]$, and considers low concordance for values under 0.9 [18]. In Table 1, we show the concordance results obtained for the emphysema (lower diagonal) and FSAD (upper diagonal). We highlighted values under 0.9 of concordance to enhance the methods that can provide further information compared to the original image. Note that all of the reference methods show an almost exact concordance with the original image and among them. This implies that all the reference methods do not provide further information compared to the original image. The harmonized data, however, shows a lower concordance, suggesting that the emphysema and FSAD description can be improved. Indeed, in the next section, we demonstrate that the harmonized data allows us to distinguish better the interplay between FSAD and emphysema that leads to a better description of functional respiratory outcomes.

Table 1. Concordance correlation coefficients for the PRM metrics: Emphysema% (lower diagonal) and FSAD% (upper diagonal). Low concordance (<0.9) is highlighted with bold letters. The low concordance for emphysema and FSAD of the harmonized image shows that the harmonized data is the only one providing different information about FSAD and emphysema from the one obtained in the original image.

	Original	NLM	Median1	Median2	Harmonized
Original	-	0.99	0.98	0.96	**0.84**
NLM	1.00	-	1.00	0.98	**0.80**
Median1	1.00	1.00	-	1.00	**0.77**
Median2	0.99	1.00	1.00	-	**0.72**
Harmonized	**0.88**	**0.86**	**0.85**	**0.83**	-

Physiological Validation. The common histological references for emphysema and small airway disease are the mean linear intercept and the airway counting approach [1]. However, when histological approaches are not available, indirect functional measures must be used. An indirect validation is usually performed by evaluating the ability of the measurements obtained with each approach to ascertain the physiological response to emphysema and small airway disease. Both processes imply a reduction in lung function due to airway collapse (emphysema) and increase airway resistance (small airway disease) that can be assessed

Table 2. Linear regression analysis for the FEV1% with respect to the amount of emphysema (Emph%) and small airway disease (FSAD%).

	Original $R^2 = 0.51$		**NLM** $R^2 = 0.50$		**Median1** $R^2 = 0.47$		**Median2** $R^2 = 0.45$		**Harmonized** $R^2 = \mathbf{0.54}$	
	Beta	p-value	Beta	p-value	Beta	p-value	Beta	p-value	Beta	p-value
Emph%	0.03	0.95	0.08	0.88	0.03	0.94	0.07	0.89	**-0.72**	<0.001
FSAD%	**-1.93**	<0.001	**-1.88**	<0.001	**-1.73**	<0.001	**-1.63**	<0.001	**-1.19**	<0.001

by the Force Expiratory Volume in 1-second percent predicted (FEV1%). We show in Table 2 the results of the multivariate linear models that relate Emph% and FSAD% to FEV1% for each method. Note that the reference methods obtain the same outcome as the one obtained with the original image: a significant effect of FSAD% in the FEV1%. However, note also that the explained variance is lower for all the reference cases. This result shows that the commonly used noise reduction methods do not provide a better description of FSAD and emphysema interplay. On the other hand, the harmonization improves the explained variance from 51% to 54%, showing that the harmonized data contributes to model the lung function better than the original image and any reference method. Furthermore, with the harmonization, the emphysema becomes statistically significant, showing a negative relationship of the emphysema ratio with the lung function. This result is consistent with the natural progression of COPD: "the function declines as both the emphysema and FSAD ratios increase," and exhibits the importance of the proposed harmonization technique in distinguishing FSAD and emphysema.

4 Conclusion

We have presented a harmonization technique to deal with non-stationary noise and bias in chest CT scans. Our approach rests on a mixture model that describes the local statistics of the CT signal. The model is used to stabilize the noise and generate a stationary process. Then, the spatially varying bias induced by noise is corrected by removing the linear dependence between the signal and the noise variance. Finally, the systematic bias is removed by adjusting with trachea and aorta reference levels. This approach was used in the quantification of both emphysema and small airway disease using the PRM methodology. This is an ideal problem to illustrate our approach as it deals with information from two images acquired at inspiration and expiration with different noise characteristics due to acquisition and lung volume differences. The assessment is performed through a population study of 48 subjects acquired from different scanners and manufacturers. Comparisons with other reference methods show that the CT harmonization provides a significant increase in the detection of both emphysema and airway disease when compared to the original image or the reference methods. This increase results in a better distinction between emphysema and

airway disease that cannot be achieved with the PRM analysis in the original image or the image filtered with the reference methods, as the concordance analysis confirmed. Additionally, the better distinction between emphysema and airway disease significantly increases the correlation with functional metrics of airway obstruction suggesting that our approach is better empowered to measure biomarkers that better reflect the disease pathophysiology.

References

1. Hogg, J.C., et al.: The nature of small-airway obstruction in chronic obstructive pulmonary disease. New Engl. J. Med. **350**(26), 2645–2653 (2004)
2. Müller, N.L., Staples, C.A., Miller, R.R., Abboud, R.T.: Density mask. An objective method to quantitate emphysema using computed tomography. Chest **94**(4), 782–787 (1988)
3. Coxson, H.O., Mayo, J., Lam, S., Santyr, G., Parraga, G., Sin, D.D.: New and current clinical imaging techniques to study chronic obstructive pulmonary disease. Am. J. Respir. Crit. Care Med. **180**(7), 588–597 (2009)
4. Matsuoka, S., Kurihara, Y., Yagihashi, K., Hoshino, M., Watanabe, N., Nakajima, Y.: Quantitative assessment of air trapping in chronic obstructive pulmonary disease using inspiratory and expiratory volumetric MDCT. Am. J. Roentgenol. **190**(3), 762–769 (2008)
5. Galbán, C.J., et al.: Computed tomography-based biomarker provides unique signature for diagnosis of COPD phenotypes and disease progression. Nature Med. **18**(11), 1711–5 (2012)
6. Vaishnav, J.Y., Jung, W.C., Popescu, L.M., Zeng, R., Myers, K.J.: Objective assessment of image quality and dose reduction in CT iterative reconstruction. Med. Phys. **41**(7), 071904 (2014)
7. Kim, J.H., Chang, Y., Ra, J.B.: Denoising of polychromatic CT images based on their own noise properties. Med. Phys. **43**(5), 2251–2260 (2016)
8. Vegas-Sánchez-Ferrero, G., Ledesma-Carbayo, M.J., Washko, G.R., San José Estépar, R.: Statistical characterization of noise for spatial standardization of CT scans: enabling comparison with multiple kernels and doses. Med. Image Anal. **40**, 44–59 (2017)
9. Choi, S., Hoffman, E.A., Wenzel, S.E., Castro, M., Lin, C.L.: Improved CT-based estimate of pulmonary gas trapping accounting for scanner and lung-volume variations in a multicenter asthmatic study. J. Appl. Physiol. **117**(6), 593–603 (2014)
10. Kim, S.S., et al.: Improved correlation between CT emphysema quantification and pulmonary function test by density correction of volumetric CT data based on air and aortic density. Eur. J. Radiol. **83**(1), 57–63 (2014)
11. Vegas-Sánchez-Ferrero, G., Ledesma-Carbayo, M.J., Washko, G.R., Estépar, R.S.J.: Autocalibration method for non-stationary CT bias correction. Med. Image Anal. **44**, 115–125 (2018)
12. Chen-Mayer, H.H., et al.: Standardizing CT lung density measure across scanner manufacturers. Med. Phys. **44**(3), 974–985 (2017)
13. Bhatt, S.P.: Association between functional small airway disease and FEV 1 decline in chronic obstructive pulmonary disease. Am. J. Respir. Crit. Care Med. **194**(2), 178–184 (2016)
14. Hilts, M., Duzenli, C.: Image filtering for improved dose resolution in CT polymer gel dosimetry. Med. Phys. **31**(1), 39–49 (2004)

15. Li, Z., et al.: Adaptive nonlocal means filtering based on local noise level for CT denoising. Med. Phys. **41**(1), 011908 (2013)
16. Tristán-Vega, A., García-Pérez, V., Aja-Fernández, S., Westin, C.F.: Efficient and robust nonlocal means denoising of MR data based on salient features matching. Comput. Methods Progr. Biomed. **105**(2), 131–144 (2012)
17. Lin, LIk: A concordance correlation coefficient to evaluate reproducibility. Biometrics **45**(1), 255 (1989)
18. McBride, G.: A proposal for strength-of-agreement criteria for Lin's concordance correlation coefficient. NIWA Client Rep. **45**(1), 307–310 (2005)